Active Flutter Suppression H∞ Synthesis using Multiple Models with Imposed Aeroelastic Poles

Hugo Fournier, Robin Vernay, Paolo Massioni, Minh Tu Pham, Laurent Bako

Active Flutter Suppression H_∞ Synthesis using Multiple Models with Imposed Aeroelastic Poles

Hugo Fournier *
Airbus Operations SAS, 31060 Toulouse, France and INSA Lyon, F-69100 Villeurbanne, France

Robin Vernay †
Airbus Operations SAS, 31060 Toulouse, France

Paolo Massioni‡ and Minh Tu Pham§
Univ Lyon, INSA Lyon, Université Claude Bernard Lyon 1, Ecole Centrale de Lyon, CNRS, Ampère, UMR5005, 69621 Villeurbanne, France

Laurent Bako ¶
Univ Lyon, Ecole Centrale de Lyon, INSA Lyon, Université Claude Bernard Lyon 1, CNRS, Ampère, UMR5005, 69130 Ecully, France

A novel approach for robust active flutter suppression is studied in this work. Based on a structural and a linear unsteady aerodynamic models obtained by finite-element and doublet-lattice methods respectively, a hybrid identification technique is developed. It first computes a reliable poles-residues decomposition of a high-order model, in order to impose aeroelastic poles to a reduced-order model. The remaining unknown term is identified with the Loewner method. A complete control synthesis procedure based on a single closed-loop H_∞ criterion is developed, starting with an optimal actuators and sensors selection based on a genetic algorithm, to the progressive design of a robust LPV control law, that efficiently stabilizes models at a given range of velocities. These techniques are validated with parameterized reliable high-order aeroelastic models.

I. Introduction

The interaction of aerodynamics and structural dynamics can result in an instability called flutter. When a fluid flows along a surface, it applies local aerodynamic forces which lead to small deflections of the structure. In turn, this affects the fluid motion by creating a change of its direction called downwash. The fluid dynamics hence has a feedback effect on itself, resulting in the so-called aeroelastic system which accounts for this interaction. Some phenomena occurring on aircraft can only be predicted by aeroelastic analysis, such as nonlinear buffeting and limit cycle oscillations (LCO) [1]. The flutter instability happens when the increase in aircraft velocity eventually leads to certain aeroelastic modes to

*(Corresponding author) PhD Candidate, Flight Physics Department, Loads and Aeroelasticity Engineering, hugo.h.fournier@airbus.com
†Research and Development Engineer, Flight Physics Department, Loads and Aeroelasticity
‡Associate Professor
§Associate Professor
¶Associate Professor

become unstable, which can be described by linear models.

In order to avoid the possibility of flutter to happen, passive solutions can be applied by modifying the aircraft design and adding masses in such a way as to increase the velocity at which flutter occurs. Another approach is to design laws that use the aircraft sensors to command the control surfaces and stabilize the aeroelastic system. This technique, known as Active Flutter Suppression (AFS), has been studied since the early 1970s [2, 3]. It is still an active research topic because of its complexity, requiring the analysis of many modes interactions, which are affected by the flight conditions. AFS also offers many possibilities, ranging from simple structured single-input-single-output (SISO) control laws [4] to Linear Parametric Varying (LPV) controllers obtained by modern synthesis methods [5]. Because of the criticality of AFS systems, simpler techniques may sometimes be preferred for their robustness.

Before reviewing the different strategies that have been considered in the AFS literature, it is worth noting that the development of a control law is strongly influenced by the aeroelastic model used for synthesis, which then becomes an integral part of the control strategy and should be developed with care. This has different impacts on the control design process. First, some synthesis methods rely on certain hypotheses of the aeroelastic model such as linearity, or, as will be seen below, certain assumptions about the dependence upon the aircraft velocity. Hence, a synthesis method must be chosen with full knowledge of the simplifying assumptions it implies on the aeroelastic model. Second, some techniques can be valid for a simple model (such as a 2D beam with few degrees of freedom) and become obsolete when applied to industrial applications involving a higher complexity, which cannot be reduced without losing key information.

The main difficulty in AFS synthesis is to define control strategies that stabilize the aeroelastic system over a range of aircraft velocities, which affect the dynamics in a nonlinear way. Robustness and adaptivity are then key concepts of AFS and can be obtained in different ways. A first solution is to obtain a single controller at a given airspeed with a robustness that ensures stability at other flight points (including the airspeed, Mach number) and mass configurations. Historically, this robust approach has first been employed using simple structured controllers, by using a feedback from a certain set of sensors to actuate the available control surfaces. In [6, 7], a feedback using a single accelerometer located on the wing tip has been used as input of a third-order filter to control two symmetric pairs of ailerons. The filter is designed by closed loop poles placement, with the objective of stabilizing the flutter modes as much as possible. More recently [4, 8] have used a similar method using two distinct feedback loops: one using the wing tip accelerometer and one using the pitch rate as input, to control the ailerons. In case more sensors are used, the poles placement method becomes tedious and optimization-based synthesis can be used, such as [9] in which a multi-input-multi-output (MIMO) single output feedback (SOF) controller is designed. Another popular technique for using information coming from different sensors is the Linear Quadratic Gaussian (LQG) approach, in which a stabilizing controller that minimizes a certain quadratic cost function is obtained by algebraic Riccati equations. Such a controller uses the system's states as input, and it requires an additional observer to estimate the states from the available measurements. This approach

has been implemented in [10, 11], where the variable to minimize is the derivative of the normal acceleration. More recently, the LQG method has been implemented in [12] using a reduced order aeroelastic model obtained from accurate unsteady Computational Fluid Dynamics (CFD) calculations. In [13] LQG controllers have also been used, with a particular attention on the MIMO robustness of the system, assessed with modern tools such as disk uncertainties. Finally, H_∞ synthesis is an effective method to obtain robust stabilizing controllers, as it allows the minimization of the H_∞ norm which leads more naturally to robustness than quadratic criteria. Furthermore, it leads to state-space controllers that can have more degrees of freedom than static gains for example. This method has been applied in [14, 15] by carefully selecting the airspeed at which the controller is designed, in such a way as maximizing the flutter velocity. Indeed, designing an AFS law at too high a velocity may lead to low robustness, and the obtained controller can even destabilize the system at airspeed at which is was naturally stable. In [16], a H_∞ AFS synthesis is embedded into an outer-loop optimization of the aircraft structure. Using μ synthesis is another way to provide robustness in the controller design, and allows to study the effect of parametric and dynamic uncertainties onto the aeroelastic transfer functions and the poles trajectories when the velocity varies, as done in [17].

As opposed to the robust approach, the second main strategy for stabilizing an aeroelastic system over a range of airspeeds is the design of adaptive laws. In this case, the dynamics of the controller can vary as the aircraft approaches flutter, with or without using the airspeed as an input. The most used method consists in designing control laws at different airspeed values, and interpolating them to obtain a control law as a piecewise-affine function of the velocity. This strategy has been employed in [18, 19] for example, or in [20] where H_∞ controllers computed at three different airspeeds are obtained and interpolated. This is made possible by an adequate balanced reduction of the controllers' state-spaces. In this case, the H_∞ norm of the transfer function from the ailerons angles to the modal displacement is the criterion to minimize. Other adaptive approaches consist in directly computing a LPV controller from the model, that must generally also be LPV. In [5, 21], a parametric Linear Quadratic Regulator (LQR) formulation is proposed and applied to a velocity-dependent aeroelastic model obtained by interpolation of reduced order models computed using reduced-order Proper Orthogonal Decomposition (POD) method. In [22, 23], a Linear Fractional Transformation (LFT) formulation is proposed, taking the velocity as uncertain parameters, and allowing the controller to have a rational dependence on it. An H_∞ formulation is proposed in [24] where a LPV controller with a polynomial dependence on the velocity and the air density is obtained, assuming the model follows the same dependence. Another formulation using convex optimization and Linear Matrix Inequalities (LMI) is proposed in [25].

The adaptive methods are attractive as they allow real-time adjustments to the change of the aeroelastic dynamics. However, their practical implementation is not always straightforward. The computational cost for the controller design can become prohibitive when the complexity of the system increases, and some hypotheses on the model used for synthesis can be unrealistic. Some of the most technologically advanced systems include the F-XDIA project developed by Politecnico di Milano and University of Washington that performed wind tunnels tests with a full model aircraft

[9, 13, 18, 19], or the European FlexOp project that recently performed flight test with a demonstrator [26]. A study has been conducted at Airbus in [27] with a model close to the one used in the present work, focusing on the practical implementability from an industrial point of view.

A novel strategy is developed with the objective of obtaining simple laws, that can be designed and validated with industrial aeroelastic models that include a high number of modes, and that smoothly adapt to the aircraft velocity. This is performed by first developing hybrid system identification methods where a certain number of aeroelastic poles (stable or unstable) are computed and imposed to the model thanks to an adequate pole-residues decomposition and the use of the Loewner method [28, 29]. An H_∞ synthesis is then performed based on multiple models of various airspeed values (lower and higher than the flutter velocity) in a way that imposes the stability at high velocity without making the low-velocity systems unstable. This method then yields a set of LPV controllers, which are subsequently validated with reliable high-order models calculated on a broad range of airspeed values. A systematic procedure is developed to select a reduced number of actuators and sensors based on quantitative criteria. It relies on a genetic algorithm that estimates the configuration leading to the best possible modulus margins achievable by full-order controllers.

II. Aeroelastic modeling

This section describes the aeroelastic modeling process. First, section II.A presents the characteristics of the aircraft used in this work. Then, section II.B uses the aeroelastic equations based on this aircraft and FEM and DLM models to obtain a high order state-space model. This model will serve two purposes: 1) to validate the controller in simulations and analysis at different airspeeds; 2) to compute the aeroelastic pole-residues decomposition that will be used in section II.C to identify reduced-order models for synthesis, with imposed poles.

A. The XRF1-HARW aircraft

The computations are performed with the XRF1-HARW (High Aspect Ratio Wing) model developed by Airbus and the University of Michigan for research purposes. Some of its characteristics are shown in Table 1. This model has a high aspect ratio and reduced wing torsional stiffness, so that the aeroelastic modes frequencies are relatively low and so is the flutter velocity. Several mass configurations, corresponding to different payload and fuel masses (with several possible distributions in the aircraft) are available for computations. A visual representation of the FEM model of the XRF1-HARW with two mode shapes (first bending and torsion modes) is shown in Fig. 1.

The XRF1-HARW model allows the placement of sensors such as accelerometers and gyroscopes on the aircraft structure. The model also includes a pair of elevators, a rudder, and 23 pairs of ailerons. This high number of actuators allows a study of an optimal ailerons placement, as it will be explained in III.C. The number of ailerons actually used will be limited in order to provide a realistic configuration and to reduce the AFS complexity.

Three aeroelastic modes are susceptible to create flutter instability as the velocity increases. One of them is unstable

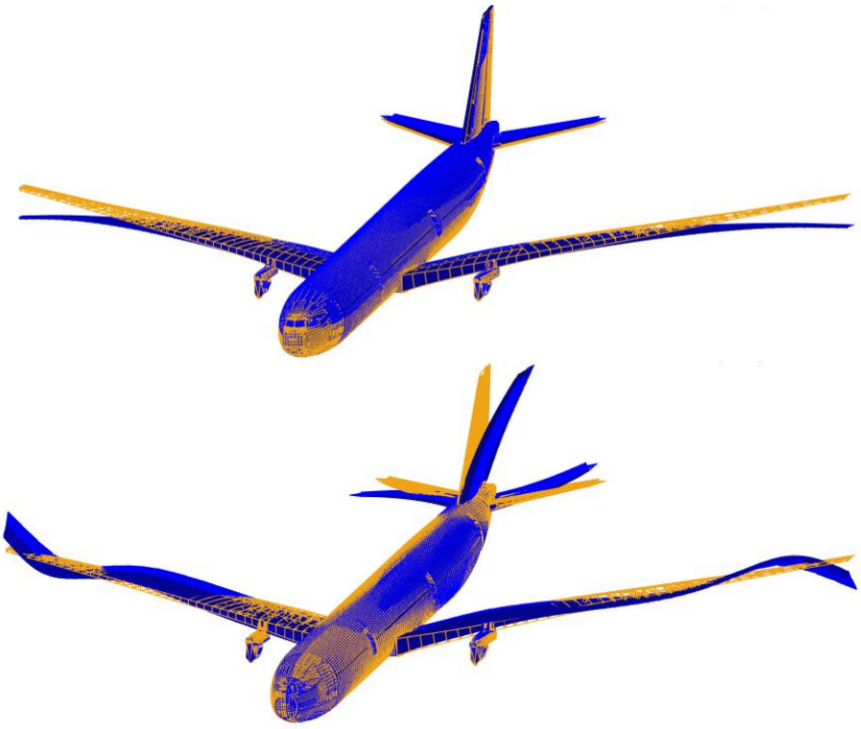

Fig. 1 First bending (up) and torsion (down) modes shapes of the XRF1-HARW

Aircraft property	Value
Wing span	70 m
Wing aspect ratio	13
Mean aerodynamic chord	7 m
Mass (min)	130.000 kg
Mass (max)	250.000 kg

Table 1 Properties of the XRF1-HAR aircraft

only in a reduced velocity range. The damping ratios of the two others keep decreasing as the velocity increases, and are then the most challenging. This has strong implications on the AFS problem studied in this work with the XRF1-HARW model: the energy cost for stabilizing the system increases with the velocity and eventually lead the actuators to reach their limits, and a trade-off must be performed between the flutter velocity we wish to impose and the actuator's capabilities.

B. High-order aeroelastic modeling

We consider the following equations describing a linearized aeroelastic system, that results from the interaction of a structural model and an aerodynamic model [1]:

$$M_{hh}\ddot{\boldsymbol{h}} + B_{hh}\dot{\boldsymbol{h}} + K_{hh}\boldsymbol{h} = \bar{q}\left[Q_{hh}(M,\kappa)\boldsymbol{h} + Q_{uh}(M,\kappa)\boldsymbol{u} + Q_{vh}(M,\kappa)\frac{\boldsymbol{v}}{V}\right] \tag{1}$$

where $\boldsymbol{h}$ is the modal displacement, $\bar{q} = \frac{1}{2}\rho V^2$ is the dynamic pressure with ρ the air density and V the aircraft true air speed, M_{hh} is the modal mass matrix, B_{hh} is the modal damping matrix, K_{hh} the modal stiffness matrix, Q_{hh}, Q_{uh} and Q_{vh} are the modal aerodynamic forces due to modal displacements $\boldsymbol{h}$, control surfaces displacements $\boldsymbol{u}$ and wind velocity $\boldsymbol{v}$ respectively. The computation is performed at different Mach numbers M and reduced frequencies $\kappa = \frac{\omega b}{V}$ with b the reference semi-chord and ω the angular frequency. This formulation includes the case where the structure and inertia of the aircraft are modeled by a finite elements model (FEM) and the aerodynamics are modeled by a linear unsteady potential theory, using for example Doublet Lattice Method (DLM) [30, 31]. From the structural, inertial and aerodynamic models, an aeroelastic solver such as sol145 of Nastran can be used to compute the matrices defining Eq. (1). Output variables of interest (integrated loads, displacements, load factors, etc) can then be obtained based on the values of $\boldsymbol{h}$, $\boldsymbol{u}$ and $\boldsymbol{v}$:

$$\boldsymbol{y} = H_y(s) \begin{bmatrix} \boldsymbol{h}^T & \boldsymbol{u}^T & \boldsymbol{v}^T \end{bmatrix}^T \tag{2}$$

where $s = j\omega$.

Because of the dependence of the generalized forces Q_{hh}, Q_{uh} and Q_{vh} on the angular frequency, the aeroelastic transfer function is not rational and cannot be transformed into a state-space system. A rational function approximation (RFA) of the aerodynamic force matrices Q_{hh}, Q_{uh} and Q_{vh} of Eq. (1) is performed by the Roger method [32]:

$$F(s) = F_0 + F_1 s + F_2 s^2 + \sum_{i=1}^{n_\gamma} \frac{F_{i+2} s}{s + \gamma_i} \tag{3}$$

where n_γ is an integer parameter, the γ_i are real strictly positive parameters called delay coefficients. These parameters are imposed by the user; a high number of delay coefficients γ_i can lead to a better approximation of the aerodynamic force matrices but increase the model's order.

Once the generalized forces Q_{hh}, Q_{uh} and Q_{vh} have been approximated by functions of the type of Eq. (3), possibly with different orders and parameters, they are replaced in the aeroelastic Eq. (1) to form a rational transfer function from control surfaces displacements $\boldsymbol{u}$ and wind velocity $\boldsymbol{v}$ to outputs of interest $\boldsymbol{y}$. In this work, the wind input is not used and the output vector contains only accelerations at different locations of the aircraft structure, and the rotation rates at the center of gravity. The matrices of the hence obtained approximate aeroelastic equations can then be assembled to form a reliable state-space model, of very high order (a few hundreds):

$$\begin{cases} \dot{\boldsymbol{x}}(t) = A\boldsymbol{x}(t) + B\boldsymbol{u}(t) \\ \boldsymbol{y}(t) = C\boldsymbol{x}(t) + D\boldsymbol{u}(t) \end{cases} \tag{4}$$

where $\boldsymbol{x}$ is the state vector, and $A \in \mathbb{R}^{n \times n}$, $B \in \mathbb{R}^{n \times N_u}$, $C \in \mathbb{R}^{N_y \times n}$ and $D \in \mathbb{R}^{N_y \times N_u}$ are matrices defining the model.

C. ROM identification with imposed aeroelastic poles

An efficient way to obtain a reduced order aeroelastic model consists in first computing the frequency response of the aeroelastic transfer function obtained in the previous section. A frequency-based system identification such as the Loewner method [28, 29] can then be applied to obtain a state-space with prescribed order. This method was used for Gust Load Alleviation (GLA) in [33, 34], and led to state-space models of order around 50 with good approximation of the frequency response in the considered range. This is well-suited for GLA in which the frequency response of a model is its most important characteristic. For AFS, the location of the aeroelastic poles is a major concern, as its main objective is to stabilize the unstable poles and to maintain the stability (possibly with certain margins) of the others. Frequency based identification techniques such as the Loewner method [28, 29] give a good approximation of the frequency response but do not guarantee that the poles are correctly modeled. A typical issue with such techniques is the fact that the identified model can be unstable even when the true system is stable. In our case, the aeroelastic poles must be correctly modeled, whether they are stable or unstable.

To this aim, we propose a novel strategy, that takes advantage of the reduced-order estimation capability of the Loewner method, while accurately imposing the aeroelastic poles. We first perform a pole-residues decomposition of the full-order aeroelastic state-space model's transfer function obtained in section II.B, assuming that each pole is simple:

$$H(s) = \sum_{i=1}^{N} \frac{R_i}{s - \lambda_i} \tag{5}$$

where the $R_i \in \mathbb{C}^{N_y \times N_u}$ are matrices called residues associated to the poles λ_i. By putting the aeroelastic state-space system (4) in the basis in which the matrix A is diagonal (which is possible because the poles are assumed to be of multiplicity 1), the R_i would be the product of a column of C and a row of B, which shows that their rank is equal to 1. However, as the matrix A is of very high order, its diagonalization is not numerically efficient. An effective solution to compute the residues is to evaluate the transfer function $(s - \lambda_i)H(s)$ at $s = \lambda_i$, which directly gives the value of R_i. Efficient ways of computing the frequency response of a transfer function of high order are required do to so, like for example with Matlab's *freqresp* function.

Only the aeroelastic poles of interest are computed with the identification procedure proposed in this section. In particular, only the poles in the frequency range of interest can be computed to reduce the order of the final system. By using the fact that the transfer function has real coefficients, it can be written as:

$$H(s) = \sum_{k=1}^{N_{sel}} \frac{R_k}{s - \lambda_k} + \frac{\overline{R_k}}{s - \overline{\lambda_k}} + H_{diff}(s) \tag{6}$$

where the over line denotes the complex conjugate, N_{sel} is the number of selected aeroelastic modes and $H_{diff}(s)$ is the difference between the full transfer function and the part we wish to impose. The idea of this methodology is to

perform a model reduction of H_{diff}, by approximating it with a reduced-order state-space model. This is done here by evaluating its frequency response, and using it to identify a reduced model by the Loewner method. Note that this new model must be stable, assuming that we have included all the unstable modes in the selected set. The final reduced order state-space model with imposed poles then has the following transfer function

$$H^{ROM}(s) = \sum_{k=1}^{N_{sel}} \frac{R_k}{s-\lambda_k} + \frac{\overline{R_k}}{s-\overline{\lambda_k}} + H_{diff}^{ROM}(s) \tag{7}$$

where H_{diff}^{ROM} has been identified with the Loewner method with imposed stability. Each subsystem associated with a selected aeroelastic pole λ_k can be put in a state-space form of order 2, and the full ROM state-space with imposed poles can be obtained with block-diagonal matrix A composed of state matrices of each subsystem, and the associated B and C matrices are obtained by concatenation.

This method has the advantage of linearly decoupling the part of the system associated with the imposed poles to the part that is reduced. Furthermore, each imposed aeroelastic mode leads to an increase of the state-space order of 1, while methods based on MIMO transfer function could lead to higher orders (a MIMO transfer function of order n cannot be transformed into a state-space model of order n in general).

III. Active Flutter Suppression design

The objective of the AFS system developed in this work is to increase the flutter velocity in presence of robustness and system's constraints. Translating this objective into a control synthesis problem is not straightforward, and different strategies have been implemented, some of which were presented in the introduction section. This work adopts a robust control approach, with the H_∞ framework. Section III.A presents the objectives and methodology of the AFS synthesis developed in this work. Section III.B describes the H_∞ criterion that the controllers must minimize to achieve AFS with imposed robustness and actuators constraints. Based on this criterion, an optimal actuators and sensors selection is performed in section III.C by solving a combinatorial problem, using a genetic algorithm when the number of possible combinations is too high. In the same section, another approach for reducing the number of inputs and outputs is studied, based on the so-called inputs/outputs blending that was proposed in [35]. Finally, section III.D describes the multi-model structured H_∞ LPV synthesis used to design AFS controllers.

A. AFS objectives and employed methodology

The main objective of the AFS controller is to improve the flutter velocity as much as possible, by stabilizing the aeroelastic system when some poles become unstable. Additionally, the stability robustness of the stabilized closed loop should be maximized, and the control effort required to do so should be minimized. Furthermore, the number of sensors and actuators actually used should be as low as possible, to reduce the cost of the AFS system in view of its practical

implementation. Finally, a smooth scheme for the AFS activation is wanted, meaning that the controller's action should start at a given velocity before flutter arises, and should increase progressively as the open-loop aeroelastic system becomes more unstable.

To achieve these objectives, a LPV controller parameterized by the True AirSpeed (TAS) of the following form is progressively developed:

$$K : \begin{cases} \dot{\boldsymbol{x}}_{\boldsymbol{K}}(t) = A_K(TAS)\boldsymbol{x}_{\boldsymbol{K}}(t) + B_K(TAS)\boldsymbol{y}_{\boldsymbol{meas}}(t) \\ \boldsymbol{u}_{\boldsymbol{com}}(t) = C_K(TAS)\boldsymbol{x}_{\boldsymbol{k}}(t) + D_K(TAS)\boldsymbol{y}_{\boldsymbol{meas}}(t) \end{cases} \tag{8}$$

where $\boldsymbol{x}_{\boldsymbol{K}}$ are the controller states, $\boldsymbol{y}_{\boldsymbol{meas}}$ and $\boldsymbol{u}_{\boldsymbol{com}}$ are respectively the measured output and control input, and the matrix functions A_K, B_K, C_K and D_K defining the state-space have a polynomial dependence on the TAS. A key driver in the design of the AFS controller is its complexity, that should be as low as possible, keeping in mind its practical implementation and certification on future aircraft. For this reason, controllers of low order are developed, through the structured H_∞ synthesis that take advantage of the multiple sensors and actuators available, and of a dynamical response to ensure good performance. Reduced configurations, in which the number of controller's inputs and outputs is lowered, are studied in section III.C, following the search of a simple controller. The reasoning behind the TAS parameterization is that the aeroelastic dynamics exhibit important variations as the velocity increases. It will be shown in the results section IV that a simple LPV structure, with affine dependence of the state-space matrices on the TAS, leads to significant improvements when a progressive evolution of the system's dynamics is desired as the velocity increases and crosses its open-loop flutter value. Controllers robust with respect to the TAS variations will be investigated too. Another cause of aeroelastic dynamics variations is the evolution of the aircraft mass configuration during a flight, or between too flights. This cannot be easily parameterized by a single variable, contrarily to the TAS dependence. Developing an adaptive law for the controllers with respect to this uncertainty is not straightforward, and the robust approach is preferred in this work. Designing a LPV controller with robustness to mass variations is a computer-intensive optimization problem, and requires the tuning of different hyper-parameters by the user. For this reason, it is performed in several steps, starting by synthesizing a controller based on a single unstable model, which is used as a starting point for a LPV synthesis, as explained in section III.D. From a LPV controller designed with models at several TAS values but with the same mass configuration, it must be decided whether the robustness to other mass configurations is ensured, and if it is not, a TAS-LPV synthesis using different mass configurations can be performed. Again, using as a starting point a controller design obtained with a single mass configuration can make the synthesis easier. This controller design strategy implies arbitrarily setting a maximum velocity value at which the closed loop should be stable. The general control architecture is illustrated on Fig. 2.

The aeroelastic model is split into longitudinal and lateral dynamics, and controllers are designed separately for each of them. Longitudinal dynamics are associated to symmetrical actuators actions (ailerons and elevators), while the

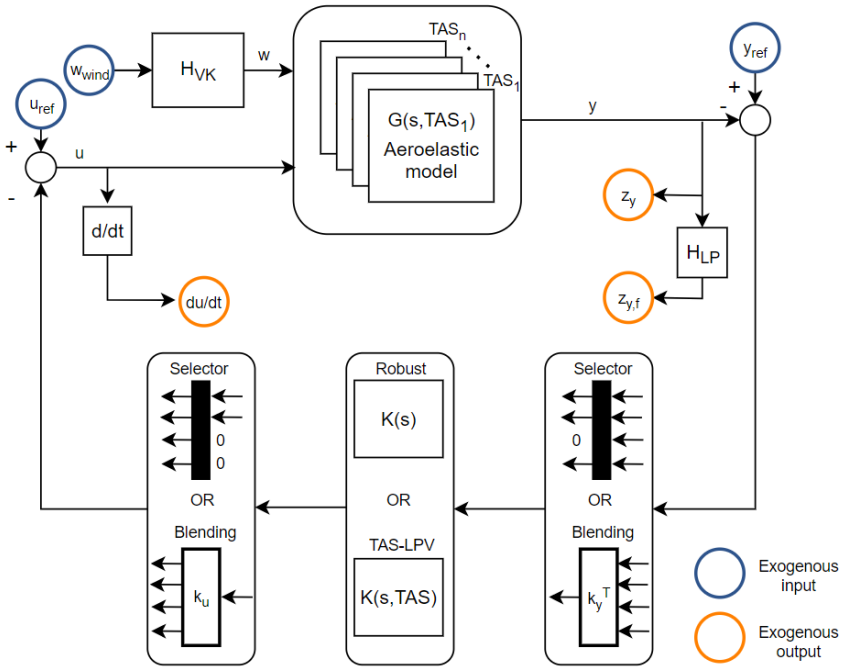

Fig. 2 General control architecture

lateral dynamics are associated to rudder deflections and antisymmetric ailerons and elevators deflections. This makes the synthesis computationally easier, and gives visibility to the AFS problem by highlighting its main bottlenecks. It will be identified that the longitudinal dynamics are much more restrictive than the lateral ones. The validation is always performed with the full dynamics, and using both controllers at the same time.

B. Synthesis criterion

Different approaches exist to translate the stabilization objectives into quantitative criteria for the controller synthesis. A first important consideration regards the models: using unstable models, such as in [20], leads to a stabilization criterion that helps satisfying the design objectives. Requiring stability of several models, such as in [18, 19], leads to a closed loop robustness criterion that, again, goes in the direction of the objectives defined above. Additionally, transfer function attenuation can be required during the synthesis, based on LQG [11] or H_∞ [20] criteria. Close to instability, the open-loop transfer function peak associated to the flutter mode increases, and imposing its attenuation in closed loop leads to damping and stability.

In this work, we impose the closed loop to be stable at a certain TAS, higher than the open-loop flutter velocity. Different cases of multi-model synthesis will be studied to improve robustness (see section III.D) and adaptivity. Additionally, four H_∞ criteria are used. The first is the limitation of the control effort, by minimizing the H_∞ norm of the transfer function from the wind velocity to the derivative of the control surfaces angle deflections. Using the wind as an input allows to bring physical information to the synthesis, by connecting the AFS problem to the main

disturbance that an aircraft can face in real applications. An input transfer is applied to the wind exogenous input so that the filter value has a Von Kármán PSD, similarly to the GLA synthesis of [33]. The derivative of the control surfaces deflections are used as output instead of the deflection angles because they are far more constraining in the technological development level of current actuators and for the relatively high frequency problem studied here (the flutter modes have a natural frequency around 4 Hz). In addition to this H_∞ constraint, two criteria are defined for MIMO robustness: the H_∞ norm of the transfer function from a reference output to the measured output must be minimized, and similarly for the input. These two transfer functions are the output and input sensitivities, and the inverse of their H_∞ norms are called the modulus margins, see [36] for instance. These margins can be related to the robustness of multiplicative inverse dynamic MIMO uncertainties [33]. Finally, a fourth criterion is added based on the transfer function from the reference output to the control surfaces deflection angles, with the inverse of a high-pass filter. This criterion helps reducing the high-frequency response of the controller, and is applied to avoid interaction with high-frequency modes.

The final H_∞ cost function to minimize is then the following scalar:

$$F(G,K) = \max \left\{ a_1 \left\| T_{w \mapsto \dot{u}} H_{VK} \right\|_\infty , a_2 \left\| T_{y_{ref} \mapsto y} \right\|_\infty , a_3 \left\| T_{u_{ref} \mapsto u} \right\|_\infty , a_4 \left\| H_{LP}^{-1} T_{y_{ref} \mapsto u} \right\|_\infty \right\} \tag{9}$$

where K is the controller, G is the aeroelastic model, H_{VK} is the Von Kármán equivalent transfer function, H_{LP} is a low-pass filter with flat response at very high frequency so that its inverse is causal, a_1 to a_4 are tuning hyperparameters, and $T_{a \mapsto b}$ designates the transfer function from a generic variable a to another generic variable b. The different signals are depicted on Fig. 2. It can be noted that the static gain of the controller $K(0)$ is not minimized here to avoid having too many constraints. Imposing $K(0) = 0$ leads to reduced interactions with handling qualities and other aeroelastic modes, and can be studied in the future.

C. Actuators and sensors selection

The full aircraft model contains many actuators and sensors described in section II.A. In order to define a realistic configuration, only some control surfaces will be used. The number of sensors used is also limited in an effort to reduce the controller's complexity. The first step to do so is to group the control surfaces: 4 sets of ailerons situated next to each other are defined on each wing, each set having approximately the same total surface. Furthermore, as explained in section III.A, the model is split into its longitudinal and lateral dynamics, and the inputs and outputs of each model are selected and modified accordingly. Two simplification of the controller are studied based on inputs/outputs selection. The first is an optimal reduction of the sensors and control surface groups used. The second, called inputs/outputs blending, is based on the work of [35]. It consists in selecting a linear combination of the inputs and of the outputs to transforms the MIMO controller synthesis into a SISO problem. The combinations are chosen in a way that maximizes the observability and controllability of a selected mode, in this case the flutter mode (as explained in section III.A, each

of the two dynamics has a problematic flutter mode whose damping continuously increases with velocity).

1. I/O selection based on closed-loop H_∞ criterion

While several criteria can be used to select the optimal inputs and outputs, such as maximizing the observability or controllability of the system, an effort is made in this work to keep the criterion as close as possible to the studied AFS synthesis problem. The objective is then to find the combination of inputs and outputs and the associated controller that minimize the H_∞ cost function defined by Eq. (9). As the number of possible combinations can be very high, this problem is very computationally expensive, especially if multi-model structured controller synthesis is performed at each iteration. For this reason, a first simplification is performed with respect to the actual synthesis described in section III.D and studied in the results by using unstructured H_∞ synthesis, compatible with the cost function of Eq. (9). As the aeroelastic models are of reduced orders, each unstructured synthesis can be performed in a limited time, and an optimal controller is obtained every time as the associated synthesis optimization is convex. The inputs and outputs selection problem hence obtained can then be formulated as:

$$\min_{\substack{u\in\mathcal{I}_u \\ y\in\mathcal{I}_y}} \min_{K} F(G_{u,y}, K) \tag{10}$$

under closed loop stability constraint, where $\mathcal{I}_u$ and $\mathcal{I}_y$ are the possible indices for the control inputs and measured outputs respectively, and $G_{u,y}$ is the aeroelastic model with only indices u and y selected in the feedback loop. In case the maximum numbers of inputs and outputs (cardinality of $\mathcal{I}_u$ and $\mathcal{I}_y$) are sufficiently low, an unstructured synthesis can be performed for each possible combination to find the optimum of this problem. However, this is generally not the case and dedicated optimization algorithms for global optimum search of a non-convex problem can be applied. In this work, a genetic algorithm [37] is used, and proves very efficient in reducing the computational cost. It starts with a population of random parameters (here the input and output indices combinations), and computes the cost function (here the maximum modulus margin obtainable by H_∞ synthesis) for each of them. It then applies a set of rules inspired from evolution to select the best candidates and obtain new ones, and repeats the process until a stopping criterion is reached. While not efficient when the parameter space dimension is important and continuous, it is an efficient technique in case only a small discrete number of parameters are possible, which is the case here. When applied with a reduced number of possible combinations, the genetic algorithm has always produced the global optimum after a few minutes, computed separately by trying all possible configurations.

2. Blending approach

Based on the work of [35], a linear combination of inputs and outputs can easily be found is order to maximize the controllability and observability of a given mode. First, by putting the state-space model of the aeroelastic system in

modal form (the matrix A is diagonal), the second-order model G_f associated to the mode of interest (two conjugate poles) can be isolated from the rest of the dynamics (G_s):

$$G(s) = G_f(s) + G_s(s) \tag{11}$$

The paper shows how to simply find the vertical vectors k_u and k_y that maximize the H_2 norm of the transfer function associated to the mode of interest:

$$\max_{\substack{\|k_u\|_2=1 \\ \|k_y\|_2=1}} \frac{\left\|k_y^T G_f k_u\right\|_2}{\left\|G_f\right\|_2} \tag{12}$$

where the norms are H_2 when applied to transfer functions and L_2 when applied to vectors. Note that the H_2 norm is infinite when the mode of interest is unstable (as in this work). In this case, the authors of [35] propose to simply mirror the real part of the unstable poles. A method to impose the resulting SISO transfer function to be decoupled from the other poles, by imposing that $\left\|k_y^T G_s k_u\right\|_2 \approx 0$, is also described, but this strongly constrains the optimization (12) and leads to an important loss of performance. For this reason, it is not applied in this work. Although this so-called blending does not reduce the number of actuators and sensors used, the analysis of the optimal blending vectors k_u and k_y provides information about which inputs and outputs are the most useful based on this modal criterion. These vectors are associated to the highest singular value of a matrix in [35]. If more singular values are kept, input and output blending matrices are obtained instead, leaving more degrees of freedom to the controller.

The two reduction techniques will be studied separately.

D. LPV multi-model H_∞ synthesis

Once the sensors and actuators have been selected or blended, the fixed-order controller can be designed in order to minimize a cost function similar to the one defined in Eq. (9). In case only one (unstable) model is used for design, the controller can be obtained by the structured H_∞ synthesis that performs the following nonlinear optimization:

$$\min_{K \in \mathcal{K}} F(G, K) \tag{13}$$

where $\mathcal{K}$ is the set of controllers K having the structure defined in section III.C, depending on the choice of inputs and outputs and on the possible multiplication by blending vectors. However, this approach does not ensure that the closed loop at lower TAS values is stable or that its performance according to the selected cost function is acceptable. To do so, a multi-model synthesis must be performed, by imposing stability at different TAS and minimizing the cost function on each of them. In this case, the cost function can depend on the TAS. The optimization associated to this multi-TAS

synthesis is:

$$\min_{K \in \mathcal{K}} \max_{i \in \mathcal{T}} F_i(G_i, K) \tag{14}$$

where $\mathcal{T}$ is the set of all TAS indices used in the controller design. It can be seen that because of how the multi-model synthesis works, only the maximum of the cost functions computed at the different TAS is minimized. If the cost functions were all minimized at the same time, a TAS-dependent criterion would not necessarily be needed. Since it is not the case, the user must define a cost function profile depending on the TAS. In this work, the cost function at a given velocity index i has the same form as the criterion defined before, but is multiplied by a coefficient b_i that makes the constraints stronger at low velocity:

$$F_i(G_i, K) = b_i F(G_i, K) \qquad i \in \mathcal{T} \tag{15}$$

A simple procedure is proposed to select these coefficients: a synthesis is performed at each index $i \in \mathcal{T}$ and the b_i are chosen as the optimal value of $F(G_i, K_i)$ found independently for each synthesis. This way, if the multi-TAS synthesis based on Eq. (14) results in a cost functions equal to 1 at each TAS value, it means that the performance is the same as the one obtained with local, independent controllers. The structure of the controller is then of particular importance, as a TAS dependence of a controller of the form of Eq. (8) can significantly improve the performance compared to a single robust controller, as explained in the results. Note that with the cost function used in this work, the best local controller obtained when the open-loop is stable is $K = 0$, which leads to no control effort and sensitivity functions equal to static identity matrix gain. The proposed methodology then encourages to obtain a controller with progressively increasing action as the TAS increases, as defined in the objectives in section III.A. In order to improve the LPV controller synthesis, the optimization can be initialized using a controller obtained with a single model.

Finally, in order to obtain robustness to mass variations, this problem can be augmented by including several models of different mass configurations at each TAS. The variation of the mass configuration is not parameterized by a single variable, contrarily to the TAS dependence. For this reason, neither the controller nor the cost function depend on it. While this methodology is implemented in this work, it does not lead to clear improvement in terms of robustness to mass variations, and the corresponding results will not be shown. Considering the Mach number, similar logics could be applied, either by defining a LPV dependence on the Mach or by imposing robustness to the dynamics variations. It is also possible to switch between different controllers that have been designed separately on a set of different Mach numbers. In this work, the Mach number is assumed constant.

IV. Results

This section presents the numerical applications of the techniques developed above with the XRF1-HARW aircraft. The numerical values of the parameters are first given in section IV.A. Then, the results of the actuators and sensors selection and of the input/output blending are described and analyzed in section IV.B. The different controller configura-

tions obtained are compared based on mono-model synthesis in section IV.C. The controller structure that leads to the best tradeoff between performance and low complexity is then retained to perform multi-model (LPV and robust logics) at different TAS values in section IV.D.

A. Parameters

The models are computed at a constant Mach number of 0.86 and an altitude of about 8000 m (which varies with the TAS). A minimum flutter velocity of 278 m/s is imposed in closed loop, meaning that the controllers syntheses will always include at least the aeroelastic model at this velocity. The longitudinal and lateral controllers have a fixed order of 5, resulting in a 10-th order full controller. The open-loop flutter velocity is about 262 m/s. The synthesis models are of 40th order, and the validation model is parameterized by the TAS and its order is about 800. The nominal mass case used in synthesis and analysis corresponds to the empty aircraft. The controllers are validated at the end of the results with four different mass configurations, that cover extreme cases of aircraft weight and center of gravity position along the X-axis (in the direction of the fuselage). In the multi-model synthesis, 7 models are used at different TAS linearly ranging from 254 m/s to 278 m/s. In the H_∞ criterion of Eq. (9), the equivalent von Kármán trubulence transfer function is

$$H_{VK}(s) = \frac{0.02s^3 + 0.3398(L_{turb}/TAS)^2 s^2 + 2.7478(L_{turb}/TAS)s + 1}{0.1539(L_{turb}/TAS)^3 s^3 + 1.9754(L_{turb}/TAS)^2 s^2 + 2.9958(L_{turb}/TAS)s + 1} \tag{16}$$

where L_{turb} is the turbulence scale, set to 762 m. The low-pass filter is a 3-rd order Butterworth filter with cut-off frequency of 6 Hz. The time simulations are performed with a vertical $1-\cos$ gust of 46 m gradient and 8.5 m/s intensity. The time simulations and root-locus are systematically obtained with the validation model. Note that some numerical values are not given due to confidentiality issues.

B. Sensors and actuators selection

The two different reduction techniques described in section III.C are studied here. In the first, we impose the controller to use 2 groups of actuators and 5 sensors for each of the longitudinal and lateral dynamics. With only one group of actuators used, the performance was strongly deteriorated and very high control effort would have been needed. Recall that the actuators candidates are four groups of ailerons, the elevators and the rudder, while the possible sensors are four accelerometers spaced along each wing's span, five accelerometers along the fuselage, one on each side of the horizontal tail plane, one on the vertical tail plane and one gyroscope at the center of gravity. In total, about 5000 configurations are possible for longitudinal dynamics and 19000 for lateral dynamics. Computing the cost function with all of them would require several hours, hence a genetic algorithm is used instead. After about 15 minutes optimization, the combination found for the longitudinal dynamics is composed of the innermost and the outermost groups of ailerons

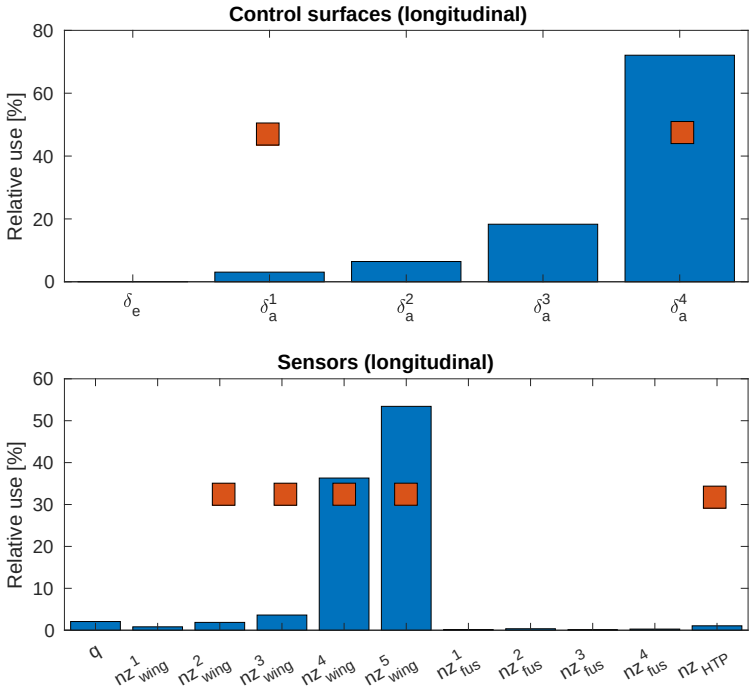

Fig. 3 Actuators and sensors selection for the longitudinal dynamics by blending vectors (blue) and H_∞-based genetic algorithm (red)

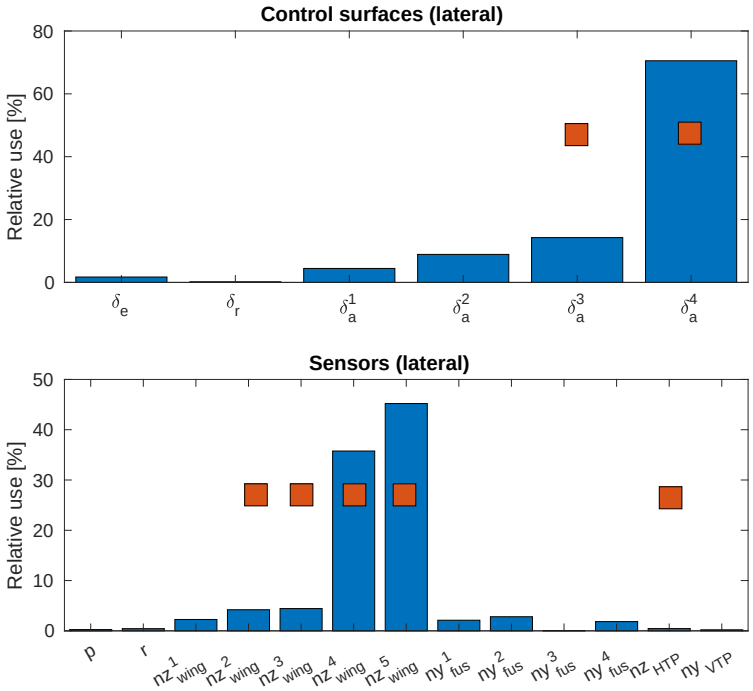

Fig. 4 Actuators and sensors selection for the lateral dynamics by blending vectors (blue) and H_∞-based genetic algorithm (red)

as actuators, and the accelerometers on the four outermost positions along the wing and at the horizontal tail plane (symmetric actions and measurements are considered for the longitudinal dynamics). Regarding the lateral dynamics, the two outermost groups of ailerons are selected, and the same sensors as for the longitudinal dynamics, but this time with antisymmetric measurements. This confirms the intuition that the actuators on the wing are the most efficient to control flutter, and in particular the outer ailerons, often used in AFS. The fact that the sensors and actuators are almost the same for the longitudinal and lateral dynamics is handy, as it limits the complexity of the full configuration. Considering that the lateral dynamics are much less constraining than the longitudinal dynamics, it is decided to use the configuration found for the former in both cases.

The second simplification, studied separately, regards the input and output blending method described in section III.C and based on the work of [35]. While the idea is different from the actuators and sensors selection analyzed above, the blending method can give hints of which inputs and outputs are the most useful following a criterion based on observability and controllability of the flutter modes. The results are summed up in Fig. 3 and 4 for the two respective dynamics. The relative use associated to each actuator/sensor obtained by blending is shown, defined as the absolute value of the blending coefficient of a signal divided by the sum of the absolute values for all signals, and the selection by genetic algorithm described above is illustrated by red squares. While the two results agree in general, the use of the innermost aileron for longitudinal dynamics, on the one hand, and of the horizontal tail plane vertical acceleration for both dynamics, on the other hand, differ. It can be explained by the fact that while the modal criterion of the blending method is restricted to the flutter mode, the H_∞ criterion used by the genetic algorithm considers the full aircraft stability. The use of the acceleration at the tail plane might not help the flutter suppression directly but be a useful information for the global stability.

C. Mono-model synthesis

Following the control design methodology described in section III.A, a structured H_∞ synthesis is first performed using a single unstable model, at $TAS = 278$ m/s. Different combinations of hyperparameters are studied in order to find an acceptable trade-off between robustness and control effort, and different controller structures are compared. This is done by simply varying the a_1 parameter of the cost function defined in Eq. (9), that regulates the control effort limitation. A controller is synthesized for 25 different linearly spaced values of a_1, and a Pareto front based on the analysis of each resulting closed loop is shown in Fig. 5. The y-axis displays the H_∞ norm of the input sensitivity function, which is the inverse of the input modulus margin. A point situated in the upper part of the figure is then less robust than a point in the lower part. For each closed loop, a time-simulation is performed with a vertical wind gust whose parameters are described in section IV.A, and the maximum control surface deflection rate is shown in the x-axis of Fig. 5. The case in which all of sensors and actuators are used is compared to the reduced configuration retained from the optimal selection and to the inputs/outputs blending of section IV.B, with one and two degrees of freedom. The two

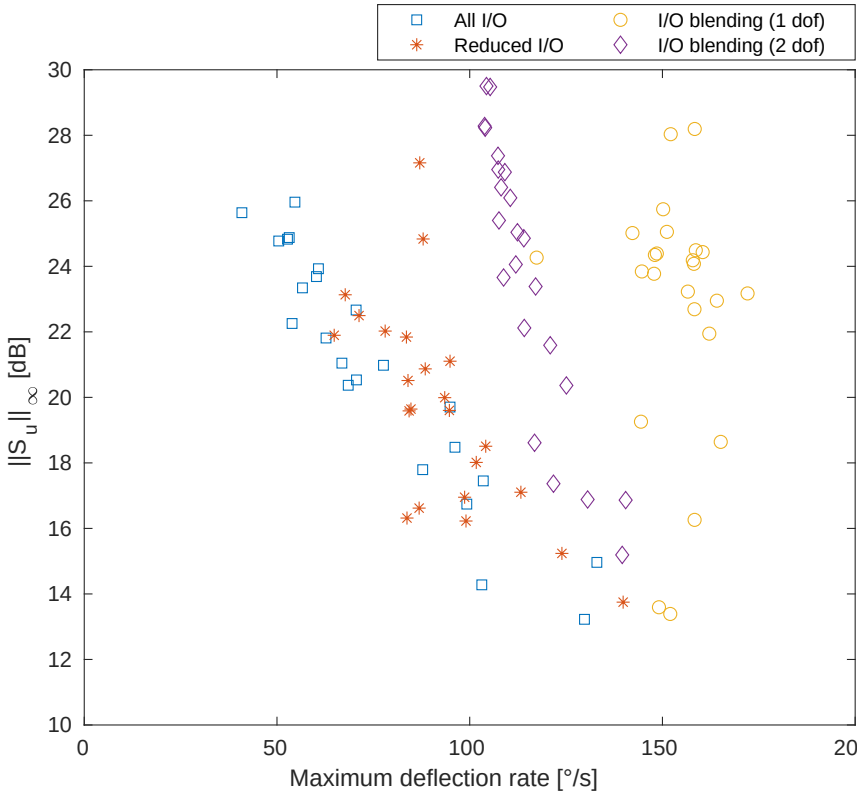

Fig. 5 Robustness/control effort Pareto front with different tuning parameters and controller structures

degrees of freedom case means that two input and two output blending vectors are used, leading to a 2×2 controller. It can be seen that, in general, the variation of the parameter a_1 leads to a trade-off between robustness and control effort. With all sensors and actuators included, maximum deflection rates as low as 50 °/s are obtained as response to a gust, which is achievable by the ailerons typically implemented on current generations of industrial aircraft. The configuration with two groups of control surfaces and five sensors (red asterisks on Fig. 5) leads to results that are very close to the full configuration. Note that, although not shown for the sake of conciseness, the performance obtained with only one group of actuators has proved significantly less good than with the full configuration. Finally, the results with inputs/outputs blending are also shown. When one degree of freedom is used, that is, the configuration where one input and one output blending vectors are used, leading to a SISO controller, the performance is significantly deteriorated compared to the full configuration of the optimal selection. When using instead two inputs and outputs vectors, which result in a reduced flutter transfer function with the same H_2 norm as the initial one (see section III.C for details), the performances are better but still less good than with the full or reduced configurations. This shows that in the case studied in this work, the criterion of expressing the unstable modes is not fully representative of the overall AFS design problem. In the end, the reduced configuration is retained for the good trade-off between controller simplicity and performance it leads to, and is used in the rest of the results. A value of a_1 leading to an input sensitivity norm of 18 dB

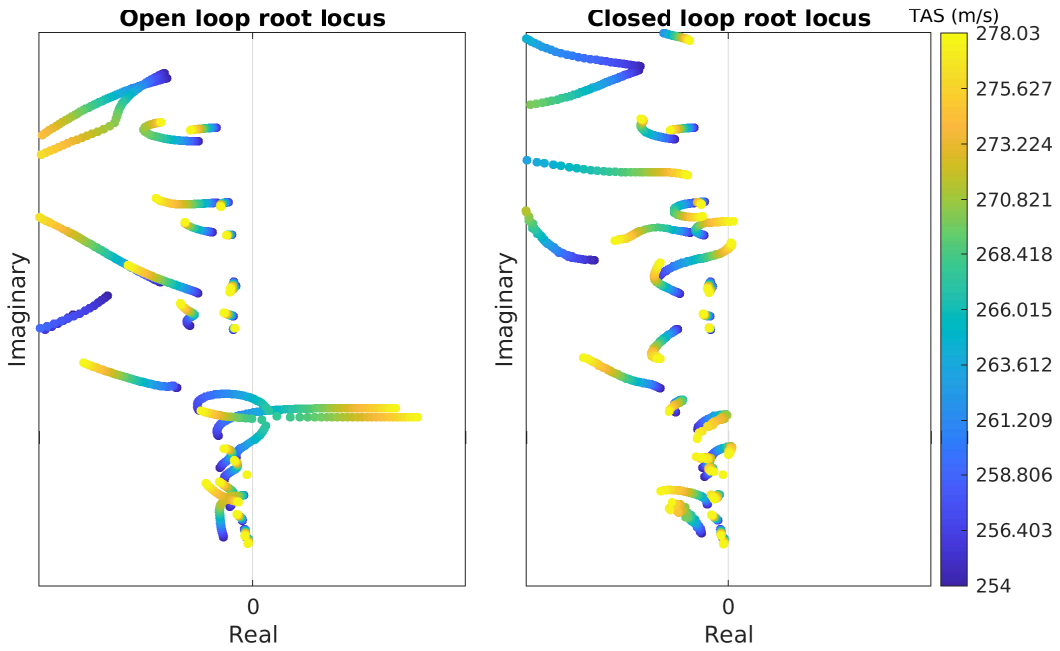

Fig. 6 Root locus at various TAS obtained with the validation model and a controller synthesized with a single model

and a maximum deflection rate of 120 °/s is selected, in order to have an acceptable robustness. While this deflection rate is typically too high to be implemented with current industrial technologies, future dedicated actuators could be able to overcome this limit. Furthermore, increasing the surface of the wing-tip ailerons that have been selected would reduce the required deflection rate.

Using the validation model, the root locus of the open loop and closed loop at different TAS values are displayed in Fig. 6. The two flutter modes with continuously decreasing damping ratio are clearly identified by they real part that becomes positive at high velocity. The third flutter mode is also seen, with a real part becoming positive and then negative again at increasing speeds. The stabilizing action of the controller leads to all modes becoming stable at velocity under 278 m/s. Note that the closed loop is globally robust to the difference between the synthesis and validation models. Furthermore, the closed loop poles location have a smooth dependence on the velocity thanks to the limitation of high-frequency controller action. However, two cases of slightly negative damping occur: one at high velocity, that means that the controller is slightly less efficient with the validation model than with the synthesis model, slightly lowering the closed loop flutter velocity. The second type of closed loop instability occurs at intermediate velocities, which is more problematic as it has a bigger impact on the flutter velocity. It means that performing the controller synthesis at one TAS is not enough. Either a more specific definition of the uncertainties the closed loop should be robust to or a better adaptivity to the change of dynamics due to the TAS variations are required. This motivates the multi-model synthesis described in section III.D, with or without TAS dependence of the controller.

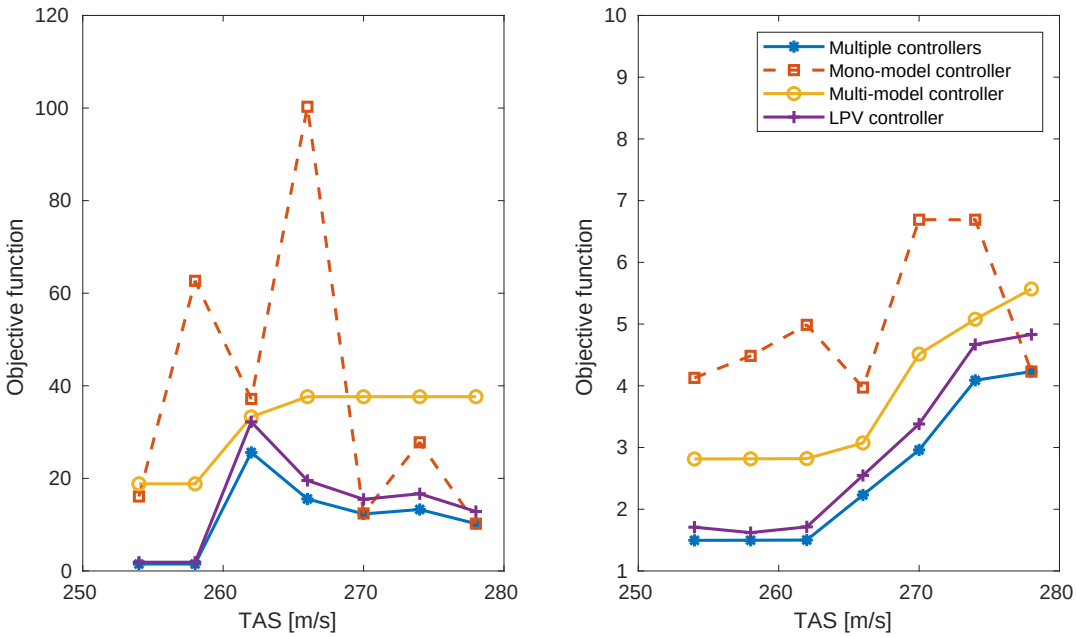

Fig. 7 Cost function obtained with different multi-TAS control designs for the longitudinal (left) and the lateral (right) dynamics

D. Multi-TAS synthesis

In order to obtain better stability and lower control effort at intermediary values of the TAS, multi-model structured H_∞ syntheses is implemented based on the method described in section III.D. The objective function computed separately on each synthesis model is shown in Fig. 7. Starting from the controller obtained with a single model in the previous section IV.C (called mono-model in Fig. 7), it can be seen that the performance at TAS values lower than the one used for design are bad, which explains the stability issue that was noted on the root locus (Fig. 6). There is no guarantee that the intermediary models are stable, hence the use of a dotted line. The first step in including intermediary models in the synthesis is done by designing a controller for each of the seven TAS values, with the same cost function. The results are given in Fig. 7 with the blue curve with asterisk markers. As expected, the cost function obtained with local controllers is better at each TAS. It is equal to 1 for models that are stable in open loop, corresponding to controller transfer functions equal to zero at all frequencies. The values of the cost function obtained for individually synthesized controllers are used as an objective profile for the synthesis of multi-model controllers, as explained in section III.D: in the best case, it will end with a multi-model cost function defined by Eq. (14) equal to one, corresponding to the same local performance as the one obtained with individual designs. The first multi-model synthesis is performed with a single robust controller, which does not depend on the TAS.

In Fig. 8, the cost functions obtained with a robust controller and using four different objective function profiles are shown. The first profile (blue solid line) is the one directly obtained from individual syntheses, and leads to bad

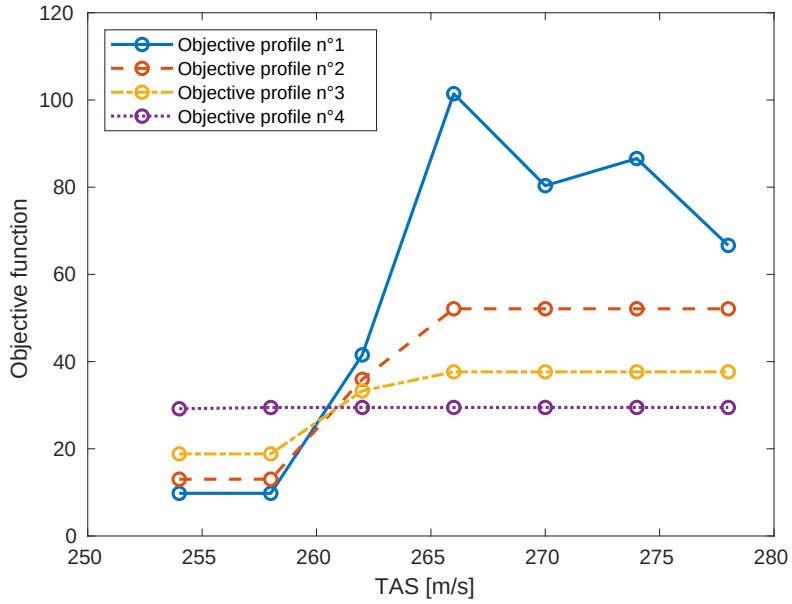

Fig. 8 Cost function obtained with robust multi-model synthesis, for different TAS-dependent objective profiles

performances at high velocity. For this reason the objective function profile can be smoothed, leading to smoother performances along the TAS profile. The other profiles are obtained by progressively diminishing the weighting difference between low and high TAS, the purple dotted line corresponding to the same weights at each TAS. Fig. 8 clearly shows the trade-off that must be made between the control performances at high and low velocities, according the criterion used in this work. The yellow curve has been selected, for the robust multi-model synthesis, and is compared to the other designs in Fig. 7. A significant deterioration of the overall control efficiency is noted when comparing the robust controller to the individual designs, demonstrating the need of an adaptation law to better follow the aeroelastic dynamics as the TAS varies. To this end, a LPV controller with affine dependence on the TAS is designed using the objective profile obtained from individual syntheses. This directly leads to good overall performances as seen on Fig. 7 with the purple line and "+" markers, that is very close to the best possible profile. In this case, a first-order polynomial dependence is enough to create the desired closed loop behavior at different velocities.

The bode diagrams of two input/output combinations of the LPV controller transfer function are shown in Fig. 9. The first combination is from the wing-tip load factor to the wing-tip symmetrical ailerons deflection, representative of the longitudinal dynamics. It can be seen that the controller amplitude starts from almost zero at the TAS which triggers the AFS system, and increases at higher velocity. The second combination regards the lateral dynamics with the same actuators and sensors but with antisymmetric action and measurement. The evolution with increasing velocity is less clear in this case, which can be explained by the fact that the lateral dynamics are less constraining than the longitudinal ones, and lower control amplitudes are required at high velocity.

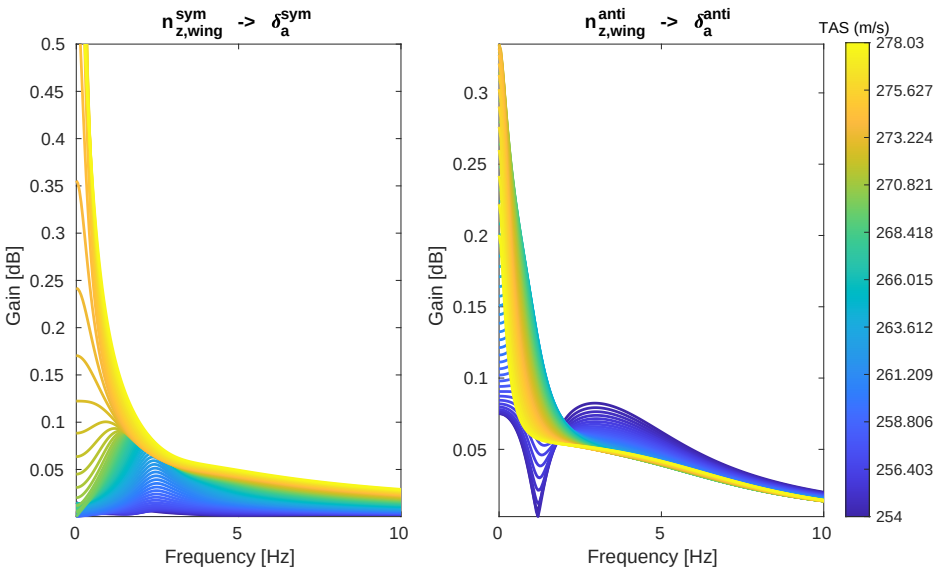

Fig. 9 LPV controller bode diagram for one longitudinal (left) and one lateral (right) transfer functions

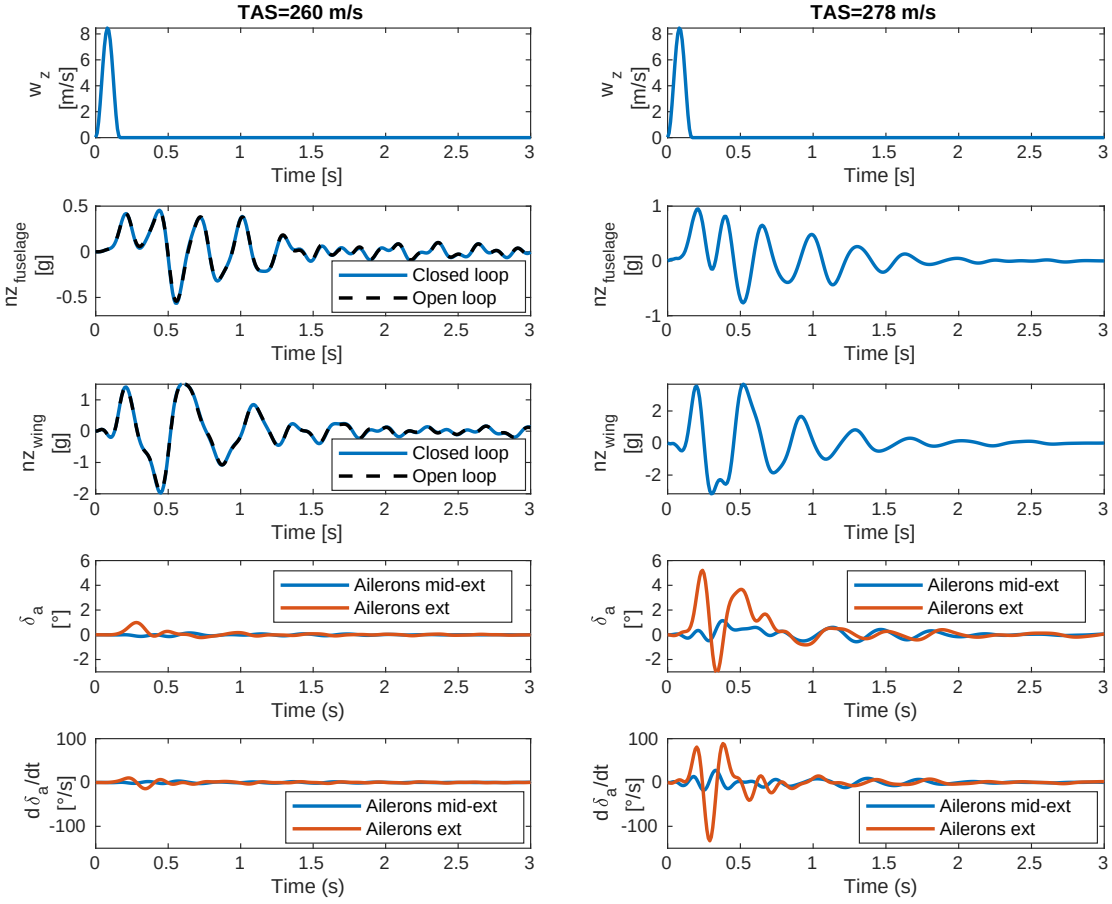

Fig. 10 Time simulations of the closed loop response to a vertical gust, using a controller with reduced number of actuators and sensors

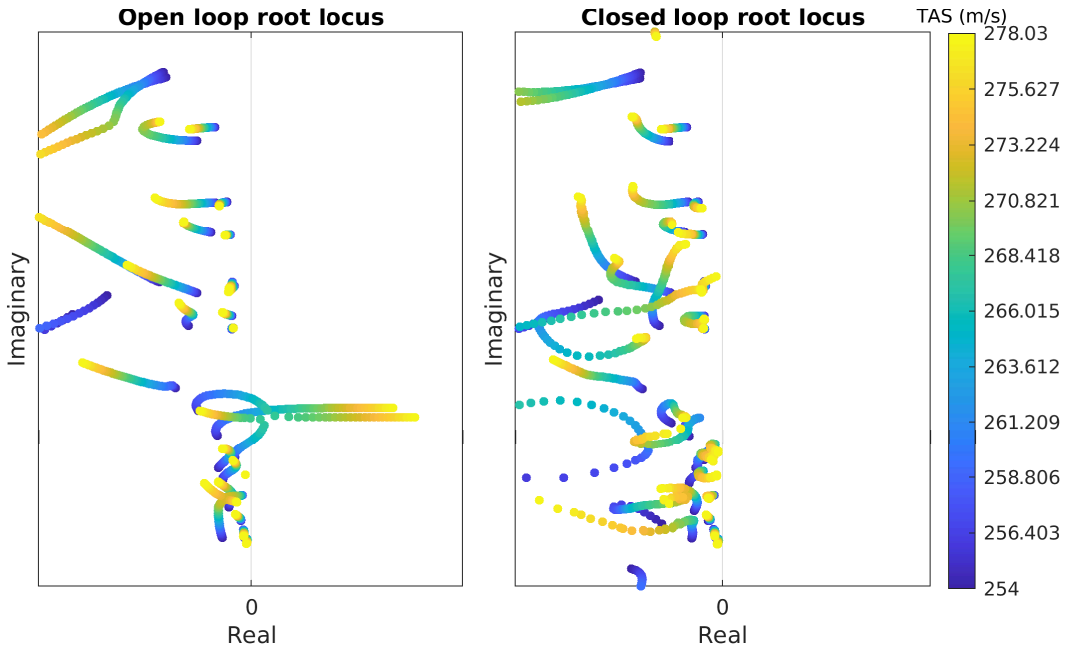

Fig. 11 Root locus at various TAS obtained with the validation model and a LPV controller

The time simulations obtained using the validation model at two values of the TAS and using the LPV controller selected from the previous considerations are shown in Fig. 10. The wind velocity w_z is displayed, followed by the vertical load factors response on the fuselage and at a location situated at the middle of the wind. At 260 m/s, the open loop is stable and can be compared to the closed loop: the objective of not disturbing the aeroelastic response at stable velocities is reached. However, the figure also shows the limit of the criterion used in this work: as no attenuation of the peak associated to the flutter modes has been required, the oscillations are not damped. The control action is low at low velocity, and reaches 120°/s at 278 m/s. The deflection angles are always lower than 10°, which is below the typical actuators constraints of the order of 30°. This also mean that no aerodynamic nonlinearity should be created from the controller's action. It can also be noted that the outer ailerons are more solicited than those that are closer to the middle of the wing. For this aircraft model, increasing the surface of the outer ailerons could then increase the AFS performances. The closed loop load factors at 278 m/s cannot be compared to the open loop case as it is unstable. It can however be seen that the fuselage load factor remains below 1 g.

Similarly to the controller that had been designed with a single model, the root loci of the closed loop obtained with the validation model and the LPV controller are plotted at different velocities in Fig. 11. This time, the real part of all modes are negative for all velocities. This confirms the interest of using a multi-model synthesis for AFS, with good multi-TAS closed-loop performances thanks to the LPV law.

Finally, an analysis of the LPV controller is performed using validation models corresponding to four mass configurations, and the results are shown in Fig. 12. As explained in section IV.A, they have been selected to cover

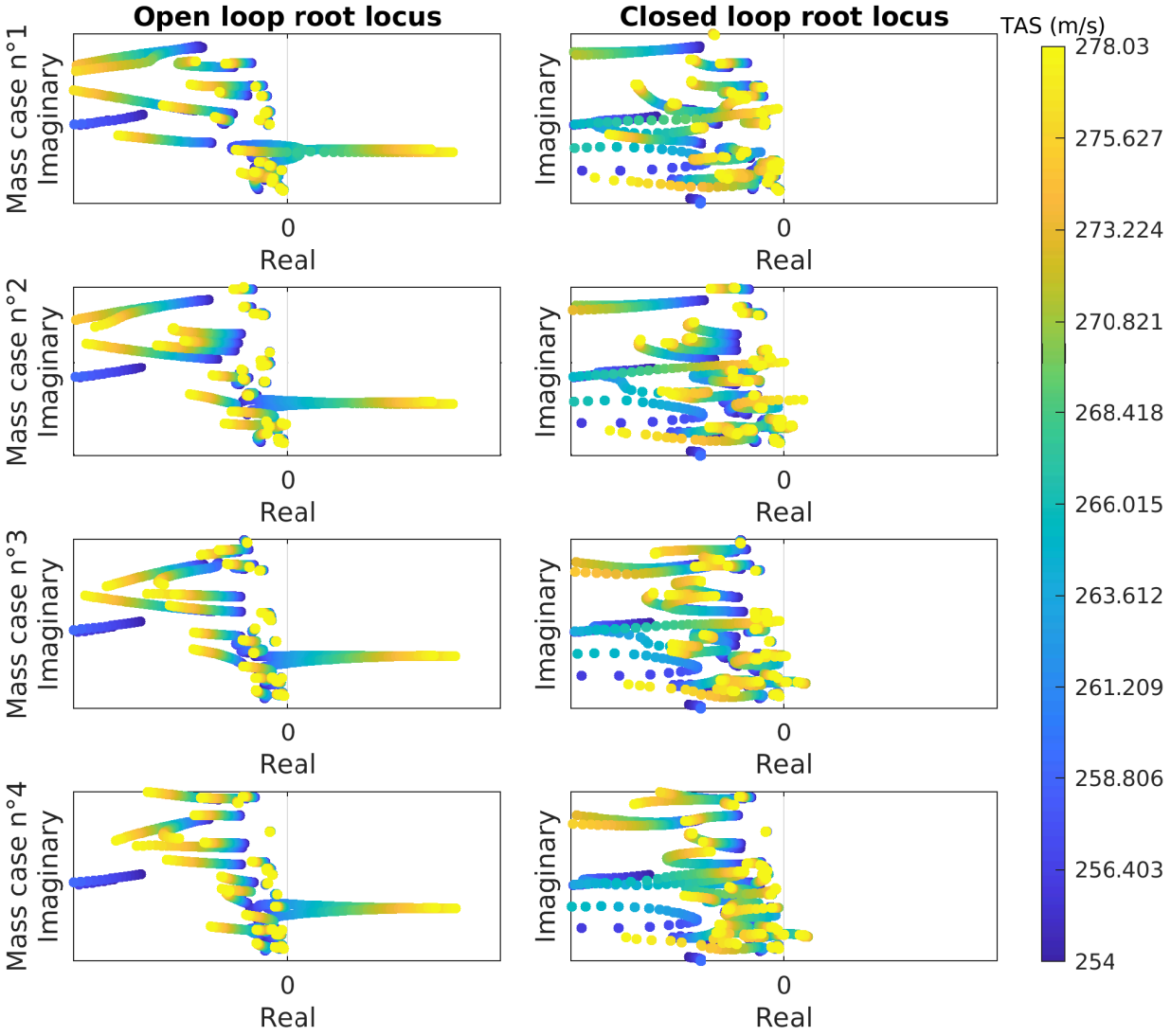
Open loop root locus
Closed loop root locus
TAS (m/s)
278.03
275.627
273.224
270.821
268.418
266.015
263.612
261.209
258.806
256.403
254
Mass case n°1
Mass case n°2
Mass case n°3
Mass case n°4
Imaginary
Real
0

Fig. 12

extreme cases of aircraft mass and center of gravity position. The first mass configuration is the same as the one used for synthesis. The global evolution of the poles shows a certain robustness to the uncertainties associated to the mass variations. While the modes are generally all stable, one of them becomes unstable in the two last mass configurations. A first solution to solve this problem could be to include in the controller design several aeroelastic models corresponding to different mass configurations. While this synthesis problem can look numerically expensive at first glance, the fact that low-order models are used with split longitudinal and lateral dynamics, and the use of initial conditions in the optimization from the LPV problem with one mass case, a control can be obtained in a few minutes. However, no improvement has been found with respect to the results shown in Fig. 12. This shows the difficulty of the AFS problem studied in this work. Not only the controller should stabilize the aeroelastic system at different velocities under important actuators constraints, but the flutter modes and their shape are susceptible to differ depending on the mass configuration. Additional research is needed to decide whether robustness to the mass configuration is possible or not, in which case adaptive laws could be required.

V. Conclusion

This work has proposed a complete control strategy for Active Flutter Suppression, starting from a hybrid reduced-order modeling of the aeroelastic system that uses frequency response data and aeroelastic modes knowledge. Based on a common objective function, an optimal sensors and actuators selection with reduced numerical complexity is proposed and different steps of controller strategy are described, form multiple mono-model syntheses at different velocities to LPV design with possible extension to multiple mass configurations. The simplicity of the controller is sought throughout this process, in the view of future industrial implementation.

The ailerons and accelerometers situated at the wing tips have been found to be the most useful for this AFS problem, using two criteria based on closed loop and observability/controllability of the flutter modes criteria respectively. However, it has been found that additional sensors and actuators are needed, probably to maintain the overall stability of the aircraft and not only the one associated to the flutter modes. The synthesis based on a single unstable model has shown its limits when validated at different velocities, and although the multi-TAS robust controller synthesis shows some improvements with respect to the former, it still leads to loss of performances compared to what can be possibly achieved with controllers designed independently at different velocities. The TAS-dependent LPV law has proved, on the contrary, very efficient, even with a simple affine dependence of the state-space matrices that constitute them on the velocity.

While these results are promising, some issues remain unsolved, such as the design of a controller valid at different mass cases and different values of the Mach number. Because of the important dependence of the aeroelastic dynamics on these parameters, a robust approach might not be sufficient and some adaptive strategy might be needed.

References

[1] Bisplinghoff, R., Ashley, H., and Halfman, R., "Aeroelasticity," Addison-Wesley Publishing Company, 1955, pp. 632–641.

[2] Nissim, E., "Flutter Suppression Using Active Controls Based on the Concept of Aerodynamic Energy," NASA TN D-6199, 1971.

[3] Sandford, M. C., Abel, I., and Gray, D. L., "Transonic Study of Active Flutter Suppression Based on an Energy Concept," *Journal of Aircraft*, Vol. 12, No. 2, 1975, pp. 72–77. https://doi.org/10.2514/3.59804, URL https://doi.org/10.2514/3.59804.

[4] Schmidt, D. K., "Stability Augmentation and Active Flutter Suppression of a Flexible Flying-Wing Drone," *AIAA Guidance, Navigation, and Control Conference*, 2016. https://doi.org/10.2514/6.2016-2099, URL https://arc.aiaa.org/doi/abs/10.2514/6.2016-2099.

[5] Chen, G., Sun, J., and Li, Y.-m., "Adaptive Reduced-Order-Model-Based Control-Law Design for Active Flutter Suppression," *Journal of Aircraft*, Vol. 49, No. 4, 2012, pp. 973–980. https://doi.org/10.2514/1.C031236, URL https://doi.org/10.2514/1.C031236.

[6] Waszak, M., and Srinathkumar, S., "Active flutter suppression - Control system design and experimental validation," *Navigation and Control Conference*, 1991. https://doi.org/10.2514/6.1991-2629, URL https://arc.aiaa.org/doi/abs/10.2514/6.1991-2629.

[7] Waszak, M., and Buttrill, C., "Design of an active flutter suppression system for the Active Flexible Wing," *Aircraft Design and Operations Meeting*, 1991. https://doi.org/10.2514/6.1991-3111, URL https://arc.aiaa.org/doi/abs/10.2514/6.1991-3111.

[8] Schmidt, D. K., "Stability Augmentation and Active Flutter Suppression of a Flexible Flying-Wing Drone," *Journal of Guidance, Control, and Dynamics*, Vol. 39, No. 3, 2016, pp. 409–422. https://doi.org/10.2514/1.G001484, URL https://doi.org/10.2514/1.G001484.

[9] Ricci, S., Marchetti, L., Riccobene, L., Gaspari, A. D., Toffol, F., Fonte, F., Mantegazza, P., Berg, J., Morgansen, K. A., and Livne, E., "An Active Flutter Suppression (AFS) Project: Overview, Results and Lessons Learned," *AIAA Scitech 2021 Forum*, 2021. https://doi.org/10.2514/6.2021-0908, URL https://arc.aiaa.org/doi/abs/10.2514/6.2021-0908.

[10] Tewari, A., "Robust optimal controllers for active flutter suppression," *Guidance, Navigation, and Control Conference and Exhibit*, 1998. https://doi.org/10.2514/6.1998-4142, URL https://arc.aiaa.org/doi/abs/10.2514/6.1998-4142.

[11] Tewari, A., "Output rate weighted active flutter suppression," *Guidance, Navigation, and Control Conference and Exhibit*, 1999. https://doi.org/10.2514/6.1999-4312, URL https://arc.aiaa.org/doi/abs/10.2514/6.1999-4312.

[12] Waite, J., Stanford, B., Bartels, R. E., and Silva, W. A., "Active Flutter Suppression Using Reduced Order Modeling for Transonic Aeroservoelastic Control Law Development," *AIAA Aviation 2019 Forum*, 2019. https://doi.org/10.2514/6.2019-3025, URL https://arc.aiaa.org/doi/abs/10.2514/6.2019-3025.

[13] Berg, J., Morgansen, K. A., Livne, E., Riccobene, L., Fonte, F., Toffol, F., Gaspari, A. D., Marchetti, L., Ricci, S., and Mantegazza, P., "Analytical and Experimental Evaluation of Multivariable Stability Margins in Active Flutter Suppression

Wind Tunnel Tests," *AIAA Scitech 2021 Forum*, 2021. https://doi.org/10.2514/6.2021-1261, URL https://arc.aiaa.org/doi/abs/10.2514/6.2021-1261.

[14] Theis, J., Pfifer, H., and Seiler, P. J., "Robust Control Design for Active Flutter Suppression," *AIAA Atmospheric Flight Mechanics Conference*, 2016. https://doi.org/10.2514/6.2016-1751, URL https://arc.aiaa.org/doi/abs/10.2514/6.2016-1751.

[15] Theis, J., Pfifer, H., and Seiler, P., "Robust Modal Damping Control for Active Flutter Suppression," *Journal of Guidance, Control, and Dynamics*, Vol. 43, No. 6, 2020, pp. 1056–1068. https://doi.org/10.2514/1.G004846, URL https://doi.org/10.2514/1.G004846.

[16] Faïsse, E., Vernay, R., Vetrano, F., Alazard, D., and Morlier, J., "Adding Control in Multidisciplinary Design Optimization of a Wing for Active Flutter Suppression," *AIAA Scitech 2021 Forum*, 2021. https://doi.org/10.2514/6.2021-0892, URL https://arc.aiaa.org/doi/abs/10.2514/6.2021-0892.

[17] Patartics, B., Lipták, G., Luspay, T., Seiler, P., Takarics, B., and Vanek, B., "Application of Structured Robust Synthesis for Flexible Aircraft Flutter Suppression," *IEEE Transactions on Control Systems Technology*, Vol. 30, No. 1, 2022, pp. 311–325. https://doi.org/10.1109/TCST.2021.3066096.

[18] Marchetti, L., Gaspari, A. D., Riccobene, L., Toffol, F., Fonte, F., Ricci, S., Mantegazza, P., Livne, E., and Hinson, K. A., "Active Flutter Suppression Analysis and Wind Tunnel Studies of a Commercial Transport Configuration," *AIAA Scitech 2020 Forum*, 2020. https://doi.org/10.2514/6.2020-1677, URL https://arc.aiaa.org/doi/abs/10.2514/6.2020-1677.

[19] Ricci, S., Toffol, F., De Gaspari, A., Marchetti, L., Fonte, F., Riccobene, L., Mantegazza, P., Berg, J., Livne, E., and Morgansen, K., "Wind Tunnel System for Active Flutter Suppression Research: Overview and Insights," *AIAA Journal (not published yet)*, 2022. https://doi.org/10.2514/1.J061985, URL https://doi.org/10.2514/1.J061985.

[20] Waitman, S., and Marcos, A., "H-infinity Control Design for Active Flutter Suppression of Flexible-Wing Unmanned Aerial Vehicle Demonstrator," *Journal of Guidance, Control, and Dynamics*, Vol. 43, No. 4, 2020, pp. 656–672. https://doi.org/10.2514/1.G004618, URL https://doi.org/10.2514/1.G004618.

[21] Chen, G., Li, Y., Jian, S., Yingtao, Z., and Hu, P., "Linear Parameter Varying Control for Active Flutter Suppression Based on Adaptive Reduced Order Model," *52nd AIAA/ASME/ASCE/AHS/ASC Structures, Structural Dynamics and Materials Conference*, 2011. https://doi.org/10.2514/6.2011-1773, URL https://arc.aiaa.org/doi/abs/10.2514/6.2011-1773.

[22] Barker, J. M., Balas, G. J., and Blue, P. A., "Gain-Scheduled Linear Fractional Control for Active Flutter Suppression," *Journal of Guidance, Control, and Dynamics*, Vol. 22, No. 4, 1999, pp. 507–512. https://doi.org/10.2514/2.4418, URL https://doi.org/10.2514/2.4418.

[23] Barker, J. M., and Balas, G. J., "Comparing Linear Parameter-Varying Gain-Scheduled Control Techniques for Active Flutter Suppression," *Journal of Guidance, Control, and Dynamics*, Vol. 23, No. 5, 2000, pp. 948–955. https://doi.org/10.2514/2.4637, URL https://doi.org/10.2514/2.4637.

[24] Moulin, B., "Robust Controller Design for Active Flutter Suppression," *AIAA Guidance, Navigation, and Control Conference and Exhibit 2004*, 2004. https://doi.org/10.2514/6.2004-5115, URL https://arc.aiaa.org/doi/abs/10.2514/6.2004-5115.

[25] Alhajjar, A. M., Al-jiboory, A., Swei, S. S.-M., and Zhu, G. G., "LPV Modeling and Control for Active Flutter Suppression of a Smart Airfoil," *2018 AIAA Guidance, Navigation, and Control Conference*, 2018. https://doi.org/10.2514/6.2018-1342, URL https://arc.aiaa.org/doi/abs/10.2514/6.2018-1342.

[26] Takarics, B., Patartics, B., Luspay, T., Vanek, B., Roessler, C., Bartasevicius, J., Koeberle, S. J., Hornung, M., Teubl, D., Pusch, M., Wustenhagen, M., Kier, T. M., Looye, G., Bauer, P., Meddaikar, Y. M., Waitman, S., and Marcos, A., "Active Flutter Mitigation Testing on the FLEXOP Demonstrator Aircraft," *AIAA Scitech 2020 Forum*, 2020. https://doi.org/10.2514/6.2020-1970, URL https://arc.aiaa.org/doi/abs/10.2514/6.2020-1970.

[27] Fischer, A., Schröder, F., and Thormann, R., "Active Flutter Suppression From an Industrial Perspective," *International Forum on Aeroelasticity and Structural Dynamics (IFASD)*, 2022.

[28] Mayo, A., and Antoulas, A., "A framework for the solution of the generalized realization problem," *Linear Algebra and its Applications*, Vol. 425, No. 2-3, 2007, pp. 634–662. https://doi.org/10.1016/j.laa.2007.03.008.

[29] Karachalios, D., Gosea, I., and Antoulas, A., "The Loewner framework for system identification and reduction," De Gruyter, 2019. https://doi.org/10.1515/9783110498967-006.

[30] Albano, E., and Rodden, W. P., "A doublet-lattice method for calculating lift distributions on oscillating surfaces in subsonic flows." *AIAA Journal*, Vol. 7, No. 2, 1969, pp. 279–285. https://doi.org/10.2514/3.5086, URL https://doi.org/10.2514/3.5086.

[31] Kalman, T. P., Rodden, W. P., and Giesling, J. P., "Application of the Doublet-Lattice Method to Nonplanar Configurations in Subsonic Flow," *Journal of Aircraft*, Vol. 8, No. 6, 1971, pp. 406–413. https://doi.org/10.2514/3.59117, URL https://doi.org/10.2514/3.59117.

[32] Roger, K., "Airplane Math Modeling Methods for Active Control Design," *AGARD-CP-228*, 1977, pp. 1–11.

[33] Fournier, H., Massioni, P., Tu Pham, M., Bako, L., Vernay, R., and Colombo, M., "Robust Gust Load Alleviation of Flexible Aircraft Equipped with Lidar," *Journal of Guidance, Control, and Dynamics*, Vol. 45, No. 1, 2022, pp. 58–72. https://doi.org/10.2514/1.G006084, URL https://doi.org/10.2514/1.G006084.

[34] Fournier, H., Massioni, P., Pham, M. T., Bako, L., Vernay, R., and Colombo, M., "Robust Gust Load Alleviation at Different Flight Points and Mass configurations," *AIAA SCITECH 2022 Forum*, 2022. https://doi.org/10.2514/6.2022-0285, URL https://arc.aiaa.org/doi/abs/10.2514/6.2022-0285.

[35] Pusch, M., and Ossmann, D., "Blending of Inputs and Outputs for Modal Velocity Feedback," *2019 27th Mediterranean Conference on Control and Automation (MED)*, 2019, pp. 530–535. https://doi.org/10.1109/MED.2019.8798491.

[36] Skogestad, S., *Multivariable feedback control : analysis and design*, Wiley, Chichester New York, 1996, pp. 40–62.

[37] Goldberg, D. E., "Genetic and evolutionary algorithms come of age," *Communications of the ACM*, Vol. 37, No. 3, 1994, pp. 113–120. https://doi.org/10.1145/175247.175259.